# Reproduction of the Charge Density Wave Phase Diagram in 1$T$-$TiSe_2$ Exposes its Excitonic Character

Chuan Chen,[1,2] Bahadur Singh,[1,2] Hsin Lin,[3] and Vitor M. Pereira[1,2,*]
[1]*Centre for Advanced 2D Materials and Graphene Research Centre, National University of Singapore, Singapore 117546*
[2]*Department of Physics, National University of Singapore, Singapore 117542*
[3]*Institute of Physics, Academia Sinica, Taipei 11529, Taiwan*

(Received 9 May 2018; published 29 November 2018)

Recent experiments suggest that excitonic degrees of freedom play an important role in precipitating the charge density wave (CDW) transition in 1$T$-$TiSe_2$. Through systematic calculations of the electronic and phonon spectrum based on density functional perturbation theory, we show that the predicted critical doping of the CDW phase overshoots the experimental value by 1 order of magnitude. In contrast, an independent self-consistent many-body calculation of the excitonic order parameter and renormalized band structure is able to capture the experimental phase diagram in extremely good qualitative and quantitative agreement. This demonstrates that electron-electron interactions and the excitonic instability arising from direct electron-hole coupling are pivotal to accurately describe the nature of the CDW in this system. This has important implications to understand the emergence of superconductivity within the CDW phase of this and related systems.

DOI: 10.1103/PhysRevLett.121.226602

The layered structure of metallic transition metal dichalcogenides (TMDs) has long made them archetypes to study the interplay between charge order, lattice instabilities, and superconductivity (SC) in both quasi- [1–6] and strictly 2D settings [7–11]. One of their common characteristics is that the SC order is stabilized within (sometimes deeply) a charge density wave (CDW) phase and the phase boundary is rather sensitive to the electronic density. 1$T$-$TiSe_2$ ($TiSe_2$, in short) is a particularly noteworthy case and will be our focus. It is a low-density semimetal that undergoes a transition to a commensurate triple-$\boldsymbol{q}$ CDW at a relatively high temperature that increases from $T_c \sim 200$ K in bulk [12], to about 240 K in monolayers [7,13]. The ordering vectors double the unit cell: $\mathbf{Q}_{\mathrm{CDW}} = 0.5(\mathbf{a}^* + \mathbf{b}^* + \mathbf{c}^*) = \Gamma L$ in the bulk [12], and $\mathbf{Q}_{\mathrm{CDW}} = 0.5(\mathbf{a}^* + \mathbf{b}^*) = \Gamma M$ in the monolayer [7,14]; the other two wave vectors are symmetric counterparts of $\mathbf{Q}_{\mathrm{CDW}}$ under $C_3$ rotations.

With no Fermi surface nesting [15] and a robust periodic lattice distortion (PLD) in tandem with the CDW [12], it is natural to consider the role played by soft phonons arising from a strong and $k$-textured electron-phonon coupling, similarly to the cases of 2$H$-$NbSe_2$ or 2$H$-$TaSe_2$ [16–18]. This would find support in density functional theory (DFT) calculations that reveal softening of an acoustic mode at $\mathbf{Q}_{\mathrm{CDW}}$ [19–21] in agreement with inelastic scattering experiments [22,23]. However, despite structural similarities, $TiSe_2$ is a fundamentally different electronic system where one expects enhanced electronic interactions: The band structure of the normal state has small overlapping electron and hole pockets offset in momentum by precisely $\mathbf{Q}_{\mathrm{CDW}}$ [24,25], which strongly hints at a possible electronic instability of the excitonic type [12,26]. Despite the long-standing theoretical prediction for the conditions under which an excitonic insulator ground state should emerge [27–29], no representative system has yet been decisively found.

Recently, inelastic x-ray measurements identified a dispersive electronic mode compatible with the development

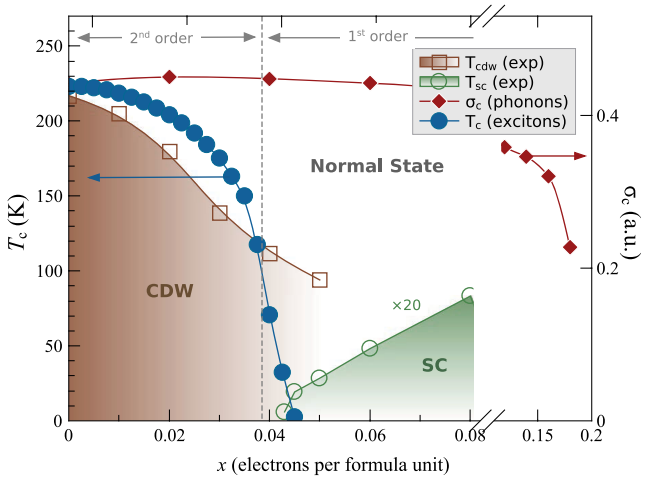


FIG. 1. Filled circles represent $T_c(x)$ obtained from the self-consistent solution of the excitonic instability. The strength of the coupling is the only adjustable parameter, and was fixed at $V = 450$ meV to yield $T_c(0) = 220$ K. The diamonds show the critical smearing parameter ($\sigma_c$) above which the phonon instability disappears (note the break in the horizontal axis). Experimental data for $T_c$ (open squares) and $T_{\mathrm{sc}}$ (open circles) were extracted from Ref. [5].

 

of an excitonic condensation at $T_c$ [30]. That excitons and interactions can be important has been increasingly better documented by a number of modeling refinements: Cercellier, Monney *et al.* showed such mechanism alone could account for a number of features observed in the evolution of the angle-resolved photoemission spectroscopy (ARPES) spectrum of undoped $TiSe_2$ [31–34] through the CDW transition; based on an approximate quasi-1D model, van Wezel *et al.* discovered that exciton condensation can enhance the lattice distortion [35,36]. Hence, the outstanding question is not whether excitonic physics is at play, but how much so.

Since the dependence of $T_c$ on electronic density is well known experimentally, we submit that the predicted density dependence of $T_c$ in a description with and without account of the excitonic mechanism should be different. As a result, it provides a direct, well-defined means to quantify the importance of excitonic condensation in the transition to the CDW phase in $TiSe_2$. Indeed, here we demonstrate that the experimental density dependence of $T_c$ in $Cu_xTiSe_2$ cannot be captured without explicitly accounting for electron-electron interactions and the excitonic instability, as summarized in the calculated phase diagram of Fig. 1.

*Excitonic instability.*—CDW order is stabilized by intralayer physics (even in bulk $TiSe_2$, Sec. S-IV [37]) which explains the strong similarity of electronic and phononic band structure changes in monolayer and bulk, as well as their doping phase diagram [5,9,13,38]. Therefore, to interrogate whether the excitonic mechanism is able to drive the system through a CDW transition in agreement with experiments, we study the $TiSe_2$ monolayer. Although there are two hole pockets [Fig. 3(a)], we consider only the highest one (Sec. S-I.D [37]), similarly to previous studies [32,33,60]. It is modeled as isotropic with $\varepsilon_{v\boldsymbol{k}} \equiv -\hbar^2\boldsymbol{k}^2/2m_v + \epsilon_{bo}$, centered at the Γ point, while the three electron pockets at each $M_i$ point have anisotropic effective masses, $\varepsilon_{c\boldsymbol{k},i} \equiv \hbar^2(\boldsymbol{k}-\boldsymbol{M}_i)_\perp^2/2m_{c,\perp} + \hbar^2(\boldsymbol{k}-\boldsymbol{M}_i)_\parallel^2/2m_{c,\parallel}$, as per Fig. 2. When undoped, the chemical potential ($\mu$) of $TiSe_2$ is placed near the intersection of the conduction and valence pockets, in agreement with the folded DFT band structure calculated in an unrelaxed $2\times 2$ superlattice [cf. Fig. 3(a)], and also tallying with transport experiments that reveal both electron and hole carriers in the normal state [5,12]. The band parameters have been extracted by fits to ARPES data in Ref. [7] in the normal state [61]. Since the bands strongly renormalize near $E_F$ and CDW fluctuations are likely present at $T \gtrsim T_c$ [32], the fitting privileged large energy ranges above and below, rather than the close vicinity of $E_F$. With these, our normal state electron density is $n_e \sim 4\times 10^{13}$ cm$^{-2}$, consistent with the experimental Hall data [12] (see also Fig. S4 in the Supplemental Material [37]).

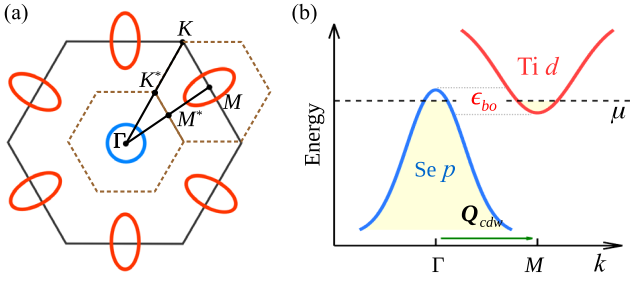


FIG. 2. (a) Schematic of the electron (Γ) and hole ($M$) pockets in the first Brillouin zone. The dashed lines highlight the folded zones in the $2\times 2$ distorted state. (b) Illustration of the indirect band overlap.

The Hamiltonian comprises these 4 "bare" bands and a *direct* Coulomb interaction between electrons at the valence and conduction pockets [27–29,32]:

$$H \equiv \sum_{\boldsymbol{k},\sigma} \varepsilon_{v\boldsymbol{k}} c^\dagger_{\boldsymbol{k},\sigma} c_{\boldsymbol{k},\sigma} + \sum_{\boldsymbol{k},\sigma,i} \varepsilon_{c\boldsymbol{k},i} d^\dagger_{i,\boldsymbol{k},\sigma} d_{i,\boldsymbol{k},\sigma} + \frac{1}{\mathcal{N}} \sum_i \sum_{\boldsymbol{k},\boldsymbol{k}',\boldsymbol{q},\sigma,\sigma'} V_{i,\boldsymbol{q}} c^\dagger_{\boldsymbol{k}+\boldsymbol{q},\sigma} d^\dagger_{i,\boldsymbol{k}'-\boldsymbol{q},\sigma'} d_{i,\boldsymbol{k}',\sigma'} c_{\boldsymbol{k},\sigma}, \quad (1)$$

Here, $c_{\boldsymbol{k},\sigma}(d_{i,\boldsymbol{k},\sigma})$ are annihilation operators for electrons at the valence ($i$th conduction) pocket with momentum $\boldsymbol{k}$ ($\boldsymbol{M}_i + \boldsymbol{k}$) and spin $\sigma$, and $\mathcal{N}$ is the number of unit cells of the crystal (for electron pockets at $\boldsymbol{M}_i$, $\boldsymbol{k}$ represents the momentum measured from $\boldsymbol{M}_i$). The chemical potential $\mu$ is implicit in $\varepsilon_{c\boldsymbol{k}/v\boldsymbol{k}}$ which are measured with respect to it. A mean-field decoupling generates the order parameter

$$\Delta_{i,\boldsymbol{k},\sigma}(T) \equiv \frac{1}{\mathcal{N}} \sum_{\boldsymbol{k}'} V_{i,\boldsymbol{k}-\boldsymbol{k}'} \langle d^\dagger_{i,\boldsymbol{k}',\sigma} c_{\boldsymbol{k}',\sigma} \rangle \quad (2)$$

that is directly related to the amplitude of the CDW at $\boldsymbol{k} = \mathbf{Q}_{\mathrm{CDW}}{}^{(i)}$ [37]. In view of the $C_3$ symmetry among the three pockets $i$ and the small pocket size, we approximate $V_{i,\boldsymbol{q}}$ and $\Delta_{i,\boldsymbol{k},\sigma}$ to $i$- and $\boldsymbol{k}$-independent constants. In particular, $\Delta \equiv \Delta_{i,\boldsymbol{k},\sigma}$ is the central quantity for our mapping of the temperature-doping phase diagram associated with the excitonic instability. It obeys a self-consistent equation [37], cf. Eq. (S8), whose solution for different $\mu$ yields the transition temperature $T_c$ to the CDW phase ($\Delta \neq 0$) as a function of doping.

*Self-consistent phase diagram.*—Figure 1 shows the resulting $T_c$, calculated entirely self-consistently at different doping for the first time, and how it compares with the experimental transition temperatures [see also Fig. S2(a)]. It can be clearly seen that (i) the decreasing trend from $x = 0$ follows very well the experimental behavior until $x \approx 0.038$, (ii) the calculation predicts $T_c \to 0$ at precisely the doping where the CDW changes from commensurate to incommensurate [62], and SC phase emerges ($x \approx 0.04$), and (iii) the transition is of second order until $x \approx 0.038$, becoming first order afterwards, which correlates with the doping for the onset of discommensurations or ICDW observed in recent experiments [37,62]. Having set all the bare band parameters from ARPES data as described earlier, our theory of the charge instability depends only on one

parameter: the coupling $V$. We set it at 450 meV to match the calculated $T_c$ to the experimental one at $x = 0$. With $V$ thus fixed, the results for $T_c$ at different $x$ shown in Fig. 1 follow without further parameters adjustment. At $x = 0$ we have $\Delta(0) \approx 25$ meV [Fig. S2(b) in the Supplemental Material [37]], in reasonable agreement (given the approximations) with ~50 meV measured in bulk and monolayer [7,60] after subtracting background fluctuations from the latter, as pointed out by Monney *et al.* [31,60].

Experimental confirmation of whether this mechanism is critical or not in driving the CDW instability in $TiSe_2$ and related TMDs can be obtained by probing $T_c$ as a function of both electron and hole doping to establish (i) whether an optimal $T_c$ exists and (ii) whether it correlates with having $\mu$ at the pocket intersection.

Note that the absence of nesting implies that the "renormalized" electronic bands in the CDW phase are only partially gapped [32] (Fig. S3). This translates into a predicted increase in the resistivity, $\rho(T)$, as soon as CDW fluctuations set in at $T \gtrsim T_c$, but persistence of the metallic nature at low temperatures; notably, holes are suppressed below $T_c$. All these features tally with measurements of thermal and electronic transport across the transition [5,12,37]. In addition, the preservation of partial electron pockets in the excitonic phase provides a Fermi sea for the development of SC beyond a threshold doping, and the coexistence of SC and CDW order, as seen experimentally [63].

These results reveal that the excitonic mechanism is able to capture correctly all the key qualitative aspects of the CDW transition and, in addition, account quantitatively very well for the experimental doping dependence of $T_c$. The agreement extends to the position of the CDW critical point that is predicted here to lie rather close to the experimental onset of the SC dome.

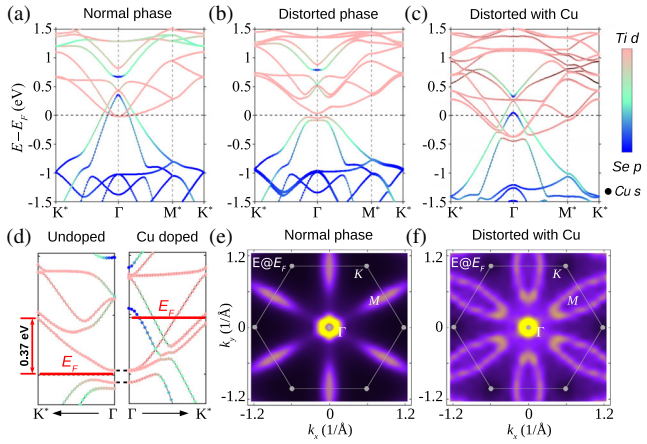


FIG. 3. Band structure obtained with a $2 \times 2$ cell in the (a) normal clamped, (b) relaxed distorted (Ti/Se atoms distort by 0.090/0.029 Å), and (c) relaxed configuration with Cu doping. See Fig. S7 of Ref. [37] for the $1 \times 1$ unfolded bands. Panel (d) presents a side-by-side close-up of (b) and (c). (e) and (f) The energy contours at $E_F$ before and after Cu doping, respectively.

*Band restructuring ab initio*.—To obtain an unbiased perspective over the doping dependence of both the reconstructed energy bands and phonon spectrum with doping, we carried out extensive DFT calculations [39] with the projector augmented wave method implemented in the Vienna *ab initio* simulation package (VASP) [40,41]. Electronic calculations used the generalized gradient approximation (GGA) [42] for the exchange-correlation functional and include spin-orbit coupling. The force constants were obtained within density functional perturbation theory (DFPT) and the phonon dispersions computed with the PHONOPY code [43,44]. Details of these calculations and methodology are given in the Supplemental Material [37]. The effects of additional carriers in $TiSe_2$ were investigated with two complementary strategies: directly simulating supercells with adsorbed Cu and by adding or removing electrons to the unit cell with a neutralizing uniform background charge.

In the high-temperature undistorted phase, $TiSe_2$ contains two Se $p$-derived hole pockets at the $\Gamma$ point slightly overlapping with three Ti $d$-derived electron pockets at the $M$ point (Sec. S-I.D.). As these are related by $\mathbf{Q}_{\mathrm{CDW}}$, in a $2 \times 2$ superlattice representation they fold to the $\Gamma$-point of the reduced Brillouin zone, as explicitly shown in Fig. 3(a). The Fermi energy ($E_F$) is slightly below the intersection of electron and hole pockets, as required by charge neutrality given the higher number of electron pockets. If one freezes the ions, these bands do not hybridize and revert to their respective primitive BZ positions in the unfolded band structure [cf. Fig. S7(b) in the Supplemental Material [37]].

Relaxing the ions yields a distorted ground state (the PLD), the overlapping pockets hybridize at $E_F$, and a gap appears ($E_g = 82$ meV) resulting in an overall lowering of energy. In addition, there is an important restructuring of the bands' shape near $E_F$ as shown in Figs. 3(b) and S5; this causes loss of the parabolic dispersion towards an inverted Mexican hat profile. In DFT, this feature was first observed in calculations only after adding GW quasiparticle corrections to the LDA band structure of bulk $TiSe_2$ [45]. Its observation here at the GGA level indicates it captures the important qualitative details to accurately describe the low density pockets in $TiSe_2$ (we discuss the electronic structure predicted with an alternative HSE hybrid functional in the Supplemental Material [37] and Fig. S6 [37]). The commensurate $2 \times 2$ PLD ground state, the magnitude of the atomic displacements, and nontrivial restructuring of energy bands are in substantial agreement with experiments. The unfolded band structure shown in Fig. S7(d) exhibits distinct back-folded bands at the $M$ point that retain the nontrivial Mexican hat shape, as has been recorded in ARPES [7,31].

*Doping by Cu intercalation*.—We now add Cu atoms to the monolayer and report in Fig. 3(c) the band structure in the reduced Brillouin zone of a fully optimized $2 \times 2$ supercell with two Cu atoms (one above and one below the

$TiSe_2$ slab, to preserve the symmetry). This visibly increases $E_F$ and restores the partial overlap between the electron and hole bands: at this doping, the system is a semimetal with a rigid upward shift of $E_F$. This is further evidenced by the Fermi contours shown in Figs. 3(e) and 3(f) that shrink at Γ and expand at $M$ to cover a large area of the BZ. Despite having been computed without and with the Cu atoms, these Fermi contours are adiabatically connected, similarly to the evolution of Fermi surfaces in the experiments [64].

There are two crucial effects of doping with Cu. First, inspection of the bands in Figs. 3(b)–3(d) shows that it does not remove the nontrivial restructuring of the dispersion near the electron-hole intersection of the pristine monolayer; Fig. 3(d) emphasizes this observation by placing the undoped and doped band structures near $E_F$ side by side. This agrees with STM measurements showing that the gap in the CDW phase of $Cu_xTiSe_2$ appears below $E_F$ and moves to higher binding energies proportionally to the Cu content [63]. Second, an analysis of atomic relaxations further reveals that doping nullifies the large atomic displacements observed in the distorted state of the undoped system and entirely suppresses the PLD (Fig. S8 [37]).

Note that the concentration of Cu in these supercell calculations is extremely high (Cu:Ti = 50%) for direct experimental comparison (the Cu solubility limit is 11% [5,46]). The crucial factor here is that, *despite* such high doping, our results provide clear evidence that the leading effect of Cu adsorption is to donate carriers to the conduction bands (one electron per Cu). This rigidly shifts $E_F$ without marked modification of the dispersion and one naturally expects a more dilute scenario to introduce even less perturbation beyond shifting $E_F$. Therefore, in order to scrutinize in detail the phonon instability at experimentally compatible doping (below 10%), we resort to the second doping strategy mentioned above, which would otherwise require prohibitively large supercells in the DFT and phonon calculations.

*Phonon softening ab initio.*—Figure 4(a) displays the phonon spectrum of $TiSe_2$ in the normal (1 × 1) phase. The

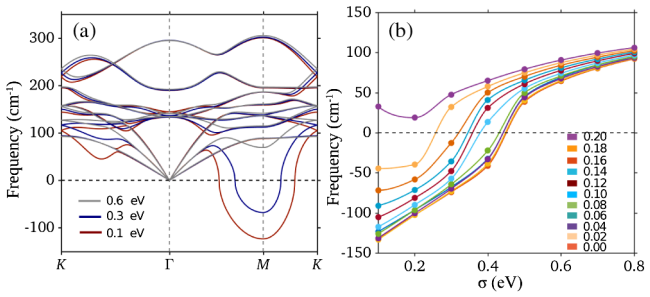


FIG. 4. (a) Phonon spectrum of the 1 × 1 normal phase with different smearing parameter $\sigma$ (undoped). (b) Evolution of the soft mode frequency at $\boldsymbol{k} = M$ as a function of $\sigma$ (abscissas) and $x$ (legends). Imaginary frequencies are represented as negative values.

qualitative influence of temperature is probed by varying the electronic smearing parameter $\sigma$, which is normally used as a technical tool in the *ab initio* calculations to accelerate the convergence and, in certain circumstances, acquires the role of electronic temperature [37]. A marked dependence of soft modes on $\sigma$ is conventionally used to trace *qualitative* changes expected to occur in the real phonon spectrum with temperature. At the smallest smearing ($\sigma = 0.1$ eV), a soft mode with imaginary frequencies (represented as negative values) around the $M$ point signals the dynamical instability towards the 2 × 2 PLD observed experimentally below $T_c$, which is complementary to that based on total energy minimization in the 2 × 2 superlattice discussed above. The fraction of the BZ associated with imaginary frequencies decreases at higher $\sigma$ and disappears beyond a critical value $\sigma_c \approx 0.45$ eV (note that only one acoustic mode is sensitive to $\sigma$, as in experiments [22]). This hardening behavior implies that undoped $TiSe_2$ should be stable only above a threshold temperature $T_c$ because, while $\sigma_c$ cannot be directly related to $T_c$, existence of a finite $\sigma_c$ can be safely used to predict a finite $T_c$ [37]; this agrees with the experimental situation.

To probe systematically the effect of small uniform doping, we studied the phonon spectrum with different concentrations of electrons in the unit cell ($x$, measured in electrons per formula unit, FU) as outlined above. The range of imaginary frequencies gradually decreases as $x$ grows, and the soft mode becomes stable above $x_c \sim 0.18 - 0.20$ [cf. Fig. S9(b) [37]]. A summary of the dependence of $\omega(\boldsymbol{k} = M)$ on both $x$ and $\sigma$ is shown in Fig. 4(b) for electron doping. A similar progression (not shown) is found with hole doping, albeit with a smaller critical density (∼0.08 holes/FU). Hence, both electron and hole doping suppress the PLD in a $TiSe_2$ monolayer.

The variation of $\sigma_c$ with doping is included in the phase diagram of Fig. 1 for comparison. While our DFPT results correctly predict the suppression of the CDW/PLD in doped $TiSe_2$, the rate of suppression with doping is much smaller than in experiments, resulting in an order of magnitude discrepancy between the predicted and experimental $x_c$. This conclusion is robust with regards to the smearing method used [37].

*Discussion.*—We provided the first complete, self-contained theoretical description of the influence of both temperature and doping in the CDW phase diagram of $TiSe_2$ in a fully self-consistent way. The solution of the excitonic instability with doping predicts a phase diagram in very good agreement with the experimental $T_c(x)$. This is significant because our bare band structure is fixed from ARPES data, the single interaction parameter $V$ is fixed once in the undoped case, and the good agreement seen for $T_c(x)$ follows without any subsequent parameter fitting. In addition, the electron-phonon coupling can be incorporated straightforwardly in this scheme, possibly enhancing the CDW instability [37,47].

The commensurate nature of the CDW, where both amplitude and phase fluctuating modes are gapped [48,49,65,66], and the high $T_c$, generically support relying on a mean-field calculation to describe the condensed phase of this problem. However, fluctuations are likely the reason for the persistence of the spectral gap in ARPES even above $T_c$ [7,31], and for our $\Delta(0) - \Delta(T_c)$ to be 0.5 [Fig. S2(b) [37]] of that same difference in experiments for undoped $TiSe_2$ [31–33,60]. The experimental restructuring towards Mexican-hat-shaped bands, with spectral transfer affecting only low energies, indicates that the physics is well described by our mean-field decoupling scheme.

Although DFT + DFPT implementations capture the electron-phonon coupling and some level of electronic correlation, they do not account for the excitonic condensation. By not explicitly capturing this physics, the calculation is unable to describe the correct degree of phonon softening, especially because the very low density places $E_F$ in the region where the spectrum is non-trivially restructured. This sensitivity to electronic interactions tallies with previous evidence that DFT-based results for the stability of the PLD and renormalized band structure depend strongly on the exchange and correlation functional, the usage of a local or nonlocal density approximation, and quasiparticle corrections [21,45,67–69].

Our results place the excitonic instability as a decisive element in the microscopic description of the CDW/PLD transition, as hinted by recent experiments that unveiled hybridized excitonic and phonon modes [30]. The current ability to map the phase diagram in strictly 2D $TiSe_2$ by gate doping [9] should allow forthcoming studies of the yet unexplored hole-doped regime, e.g., whether an optimal $T_c$ correlates with $E_F$ at the intersection of the electron and hole pockets, as predicted here.

We thank Lei Su and A. H. Castro Neto for fruitful discussions. V. M. P. was supported by the Singapore Ministry of Education through Grant No. MOE2015-T2-2-059. Numerical computations were carried out at the HPC facilities of the NUS Centre for Advanced 2D Materials, supported by the National Research Foundation of Singapore under its Medium-Sized Centre Programme.

*Corresponding author.
vpereira@nus.edu.sg

[1] J. A. Wilson, Phys. Status Solidi **86**, 11 (1978).
[2] F. Clerc, C. Battaglia, H. Cercellier, C. Monney, H. Berger, L. Despont, M. G. Garnier, and P. Aebi, J. Phys. Condens. Matter **19**, 355002 (2007).
[3] K. Rossnagel, J. Phys. Condens. Matter **23**, 213001 (2011).
[4] A. F. Kusmartseva, B. Sipos, H. Berger, L. Forró, and E. Tutiš, Phys. Rev. Lett. **103**, 236401 (2009).
[5] E. Morosan, H. Zandbergen, B. Dennis, J. Bos, Y. Onose, T. Klimczuk, A. Ramirez, N. Ong, and R. Cava, Nat. Phys. **2**, 544 (2006).
[6] Y. I. Joe, X. M. Chen, P. Ghaemi, K. D. Finkelstein, G. a. de la Peña, Y. Gan, J. C. T. Lee, S. Yuan, J. Geck, G. J. MacDougall, T. C. Chiang, S. L. Cooper, E. Fradkin, and P. Abbamonte, Nat. Phys. **10**, 421 (2014).
[7] P. Chen, Y. H. Chan, X. Y. Fang, Y. Zhang, M. Y. Chou, S. K. Mo, Z. Hussain, A. V. Fedorov, and T. C. Chiang, Nat. Commun. **6**, 8943 (2015).
[8] A. W. Tsen, B. Hunt, Y. D. Kim, Z. J. Yuan, S. Jia, R. J. Cava, J. Hone, P. Kim, C. R. Dean, and A. N. Pasupathy, Nat. Phys. **12**, 208 (2016).
[9] L. J. Li, E. C. T. O'Farrell, K. P. Loh, G. Eda, B. Özyilmaz, and A. H. Castro Neto, Nature (London) **529**, 185 (2016).
[10] X. Xi, Z. Wang, W. Zhao, J.-H. Park, K. T. Law, H. Berger, L. Forró, J. Shan, and K. F. Mak, Nat. Phys. **12**, 139 (2016).
[11] X. Xi, H. Berger, L. Forró, J. Shan, and K. F. Mak, Phys. Rev. Lett. **117**, 106801 (2016).
[12] F. J. Di Salvo, D. E. Moncton, and J. V. Waszczak, Phys. Rev. B **14**, 4321 (1976).
[13] P. Goli, J. Khan, D. Wickramaratne, R. K. Lake, and A. A. Balandin, Nano Lett. **12**, 5941 (2012).
[14] X.-Y. Fang, H. Hong, P. Chen, and T.-C. Chiang, Phys. Rev. B **95**, 201409 (2017).
[15] T. Pillo, J. Hayoz, H. Berger, F. Lévy, L. Schlapbach, and P. Aebi, Phys. Rev. B **61**, 16213 (2000).
[16] D. E. Moncton, J. D. Axe, F. J. Disalvo, E. Engineers, and E. Engineers, Phys. Rev. Lett. **34**, 734 (1975).
[17] F. Weber, S. Rosenkranz, J.-P. Castellan, R. Osborn, R. Hott, R. Heid, K.-P. Bohnen, T. Egami, A. H. Said, and D. Reznik, Phys. Rev. Lett. **107**, 107403 (2011).
[18] M. Leroux, I. Errea, M. Le Tacon, S.-M. Souliou, G. Garbarino, L. Cario, A. Bosak, F. Mauri, M. Calandra, and P. Rodière, Phys. Rev. B **92**, 140303 (2015).
[19] K. Motizuki, N. Suzuki, Y. Yoshida, and Y. Takaoka, Solid State Commun. **40**, 995 (1981).
[20] M. Calandra and F. Mauri, Phys. Rev. Lett. **106**, 196406 (2011).
[21] B. Singh, C.-H. Hsu, W.-F. Tsai, V. M. Pereira, and H. Lin, Phys. Rev. B **95**, 245136 (2017).
[22] M. Holt, P. Zschack, H. Hong, M. Y. Chou, and T. C. Chiang, Phys. Rev. Lett. **86**, 3799 (2001).
[23] F. Weber, S. Rosenkranz, J. P. Castellan, R. Osborn, G. Karapetrov, R. Hott, R. Heid, K. P. Bohnen, and A. Alatas, Phys. Rev. Lett. **107**, 266401 (2011).
[24] R. Bachrach, M. Skibowski, and F. Brown, Phys. Rev. Lett. **37**, 40 (1976).
[25] A. Zunger and A. J. Freeman, Phys. Rev. B **17**, 1839 (1978).
[26] M. M. Traum, G. Margaritondo, N. V. Smith, J. E. Rowe, and F. J. Di Salvo, Phys. Rev. B **17**, 1836 (1978).
[27] L. V. Keldysh and Y. V. Kopaev, Sov. Phys. Solid State **6**, 2219 (1965).
[28] D. Jérome, T. M. Rice, and W. Kohn, Phys. Rev. **158**, 462 (1967).
[29] W. Kohn, Phys. Rev. Lett. **19**, 439 (1967).
[30] A. Kogar, M. S. Rak, S. Vig, A. A. Husain, F. Flicker, Y. I. Joe, L. Venema, G. J. MacDougall, T. C. Chiang, E. Fradkin, J. van Wezel, and P. Abbamonte, Science **358**, 1314 (2017).

[31] H. Cercellier, C. Monney, F. Clerc, C. Battaglia, L. Despont, M. G. Garnier, H. Beck, P. Aebi, L. Patthey, H. Berger, and L. Forró, Phys. Rev. Lett. **99**, 146403 (2007).

[32] C. Monney, H. Cercellier, F. Clerc, C. Battaglia, E. F. Schwier, C. Didiot, M. G. Garnier, H. Beck, P. Aebi, H. Berger, L. Forró, and L. Patthey, Phys. Rev. B **79**, 045116 (2009).

[33] C. Monney, C. Battaglia, H. Cercellier, P. Aebi, and H. Beck, Phys. Rev. Lett. **106**, 106404 (2011).

[34] G. Monney, C. Monney, B. Hildebrand, P. Aebi, and H. Beck, Phys. Rev. Lett. **114**, 086402 (2015).

[35] J. van Wezel, P. Nahai-Williamson, and S. S. Saxena, Phys. Rev. B **81**, 165109 (2010).

[36] J. van Wezel, P. Nahai-Williamson, and S. S. Saxena, Europhys. Lett. **89**, 47004 (2010).

[37] See Supplemental Material at http://link.aps.org/supplemental/10.1103/PhysRevLett.121.226602 for additional details, which includes Refs. [5,7,9,12,13,21,23,29–33,35,36,38–59].

[38] P. Chen, Y.-H. Chan, M.-H. Wong, X.-Y. Fang, M. Y. Chou, S.-K. Mo, Z. Hussain, A.-V. Fedorov, and T.-C. Chiang, Nano Lett. **16**, 6331 (2016).

[39] P. Hohenberg and W. Kohn, Phys. Rev. **136**, B864 (1964).

[40] G. Kresse and D. Joubert, Phys. Rev. B **59**, 1758 (1999).

[41] G. Kresse and J. Furthmüller, Phys. Rev. B **54**, 11169 (1996).

[42] J. P. Perdew, K. Burke, and M. Ernzerhof, Phys. Rev. Lett. **77**, 3865 (1996).

[43] S. Baroni, P. Giannozzi, and A. Testa, Phys. Rev. Lett. **58**, 1861 (1987).

[44] A. Togo, F. Oba, and I. Tanaka, Phys. Rev. B **78**, 134106 (2008).

[45] M. Cazzaniga, H. Cercellier, M. Holzmann, C. Monney, P. Aebi, G. Onida, and V. Olevano, Phys. Rev. B **85**, 195111 (2012).

[46] G. Wu, H. X. Yang, L. Zhao, X. G. Luo, T. Wu, G. Y. Wang, and X. H. Chen, Phys. Rev. B **76**, 024513 (2007).

[47] B. Zenker, H. Fehske, H. Beck, C. Monney, and A. R. Bishop, Phys. Rev. B **88**, 075138 (2013).

[48] G. Grüner, *Density Waves in Solids* (Addison-Wesley, Reading, MA, 1994).

[49] L. Su, C.-H. Hsu, H. Lin, and V. M. Pereira, Phys. Rev. Lett. **118**, 257601 (2017).

[50] H. Bruus and K. Flensberg, *Many-Body Quantum Theory in Condensed Matter Physics: An Introduction* (Oxford University Press, Oxford, 2004).

[51] C.-W. Chen, J. Choe, and E. Morosan, Rep. Prog. Phys. **79**, 084505 (2016).

[52] D. L. Duong, M. Burghard, and J. C. Schön, Phys. Rev. B **92**, 245131 (2015).

[53] H. Frohlich, Proc. R. Soc. A **215**, 291 (1952).

[54] A. V. Krukau, O. A. Vydrov, A. F. Izmaylov, and G. E. Scuseria, J. Chem. Phys. **125**, 224106 (2006).

[55] N. D. Mermin, Phys. Rev. **137**, A1441 (1965).

[56] C. Monney, G. Monney, P. Aebi, and H. Beck, New J. Phys. **14**, 075026 (2012).

[57] D. Mou, A. Sapkota, H.-H. Kung, V. Krapivin, Y. Wu, A. Kreyssig, X. Zhou, A. I. Goldman, G. Blumberg, R. Flint, and A. Kaminski, Phys. Rev. Lett. **116**, 196401 (2016).

[58] V. Popescu and A. Zunger, Phys. Rev. B **85**, 085201 (2012).

[59] W. D. Wise, M. C. Boyer, K. Chatterjee, T. Kondo, T. Takeuchi, H. Ikuta, Y. Wang, and E. W. Hudson, Nat. Phys. **4**, 696 (2008).

[60] C. Monney, E. F. Schwier, M. G. Garnier, N. Mariotti, C. Didiot, H. Beck, P. Aebi, H. Cercellier, J. Marcus, C. Battaglia, H. Berger, and A. N. Titov, Phys. Rev. B **81**, 155104 (2010).

[61] The fit parameters are $m_v = 0.63m_e$, $m_{c,\perp} = 1.38m_e$, $m_{c,\parallel} = 3.46m_e$, $\epsilon_{bo} = 0.1$ eV (band overlap). See also Supplemental Material SIII.E.

[62] A. Kogar, G. A. de la Pena, S. Lee, Y. Fang, S. X.-L. Sun, D. B. Lioi, G. Karapetrov, K. D. Finkelstein, J. P. C. Ruff, P. Abbamonte, and S. Rosenkranz, Phys. Rev. Lett. **118**, 027002 (2017).

[63] M. Spera, A. Scarfato, E. Giannini, and C. Renner, arXiv:1710.04096.

[64] J. F. Zhao, H. W. Ou, G. Wu, B. P. Xie, Y. Zhang, D. W. Shen, J. Wei, L. X. Yang, J. K. Dong, M. Arita, H. Namatame, M. Taniguchi, X. H. Chen, and D. L. Feng, Phys. Rev. Lett. **99**, 146401 (2007).

[65] P. Lee, T. Rice, and P. Anderson, Solid State Commun. **88**, 1001 (1993).

[66] W. L. McMillan, Phys. Rev. B **16**, 4655 (1977).

[67] V. Olevano, M. Cazzaniga, M. Ferri, L. Caramella, and G. Onida, Phys. Rev. Lett. **112**, 049701 (2014).

[68] M. Calandra and F. Mauri, Phys. Rev. Lett. **112**, 049702 (2014).

[69] M. Hellgren, J. Baima, R. Bianco, M. Calandra, F. Mauri, and L. Wirtz, Phys. Rev. Lett. **119**, 176401 (2017).